RSC Advances

ROYAL SOCIETY OF CHEMISTRY

www.rsc.org/advances

Reduced Graphene Oxide-Titania based Platform for Label- Free Biosensor

Pratima R. Solanki[a,b*], Saurabh Srivastava[b,c], Md. Azahar Ali[b], Rajesh Kr. Srivastava[c], Anchal Srivastava,[c] B. D. Malhotra[b,d*]

[a] Special Centre for Nano Sciences, Jawaharlal Nehru University, New Delhi-110067, India
[b]Department of Science and Technology Centre on Biomolecular Electronics, Biomedical Instrumentation Section, CSIR -National Physical Laboratory, Dr. K.S. Krishnan Marg, New Delhi 110012, India.
[c]Department of Physics, Banaras Hindu University, Varanasi, 221005, India.
[d]Department of Biotechnology, Delhi Technical University, Shahbad Daulatpur, Main Bawana Road, Delhi-110042, India.

ABSTRACT

A label-free biosensor has been fabricated using a reduced graphene oxide (RGO) and anatase titania (antTiO_2) nanocomposite, electrophoretically deposited onto indium tin oxide coated glass substrate. The antTiO_2-RGO nanocomposite has been functionalized with proteins (horse radish peroxidase) conjugated antibodies specific recognition of *Vibrio cholerae* (Ab-*Vc*) for detection of *Vibrio cholerae*. The presence of Ab-*Vc* onto RGO-antTiO_2 nanocomposite has been confirmed using electron microscopy, Fourier transform infrared spectroscopy and electrochemical techniques. The electrochemical studies relating to the fabricated Ab-*Vc*/RGO-antTiO_2/ITO immunoelectrode have been conducted to investigate the binding kinetics. This immunosensor exhibits improved biosensing properties for detection of *Vibrio cholera* like sensitivity as 18.17×10^6 F/molL^{-1}/m^2 in the detection range of 0.12-5.4 nmol L^{-1}, and a low detection limit of 0.12 nmol L^{-1}. The association (k_a), dissociation (k_d) and equilibrium rate constants have been estimated to be as 0.07 nM, 0.002 nM and 0.41 nM, respectively. This Ab-*Vc*/RGO-antTiO_2/ITO immunoelectrode could be a suitable platform for development of compact diagnostics devices.

KEYWORDS: Proteins conjugation, reduced graphene oxide, anatase-titania, *Vibrio choleraee,* immunosensor.

*Corresponding authors: pratimarsolanki@gmail.com; bansi.malhotra@gmail.com; Tel.: +91 11 45609152; Fax: +91 11 45609312

1. Introduction

Recent advancement in nanoscience and nanotechnology has led to increased interest towards the development of the point-of-care diagnostics devices for global health, environmental monitoring and food safety.[1-4] The multifunctional nanomaterials have been found to be promising candidates for sensitive and selective detection of pathogens, smRNA, PNA, aptamer etc.[5-6] Carbon allotropes like graphene oxide (GO), fullerenes, carbon nanotubes etc. have been explored for cellular imaging, tissue engineering, intercalation materials, drug delivery biomaterials and biosensors.[7-11] For biosensor fabrication, presence of available functional groups (e.g. hydroxyl, epioxide, carbonyl, carboxyl etc.) on basal planes/edges of GO sheet may facilitate conjugation of proteins or biomolecules.[12-16] Due to its small size, intrinsic electrochemical properties, large planner area, and useful non-covalent interactions with proteins, GO is an exciting material for biomedical applications.

The electrical conductivity of GO can be tuned via chemical reduction resulting in formation of reduced graphene oxide (RGO). Compared to GO, RGO provides enhanced electrochemical properties, excellent mobility of charge carriers, and can be easily functionalized with biomolecules [14,15,17] due to its large surface area and high density of edge-plane-like defects that may allow fast heterogeneous electron transfer.[18] In addition, the ease of material processing, low cost of synthesis, mechanical flexibility of RGO may led to a wide range of applications including biosensors[18,19-20], field effect transistors,[21] photovoltaics [22] and photodetectors .[23] GO modified electrochemically pre-anodized screen-printed carbon electrodes have been developed for the determination of nicotinamide adenine dinucleotide in neutral aqueous solution.[14] The RGO has been utilized for detection of aflatoxin B1 using electrochemical technique.[24]

The metal oxide nanoparticles (MOsN) based nanocomposites with carbonaceous materials including RGO have been found to result in improved electronic properties that play a vital role for the fabrication of electrochemical biosensors.[25-28] It has been reported that the MOsN and GO nanocomposites may result in improved biosensor efficacy compared to that of using single component.[29-33] Recently, GO and titanium oxide (TiO_2) nanocomposite has been explored for the development of lithium ion battery, photocatalyst and dye sensitized solar cell.[34]

However, the RGO and MOsN composite has not yet been used for the fabrication of the electrochemical immunosensor.

Anatase TiO_2 (ant-TiO_2) is an interesting material due to its long-term stability, strong oxidizing power, low cost, biocompatibility and non-toxicity.[35] Moreover, TiO_2 nanoparticles have the ability to absorb desired proteins and provide an effective orientation for electron transfer between protein molecules and the electrode. Ali *et al*. have recently fabricated a microfluidic biochip using ant-TiO_2 nanoparticles for detection of biomolecules. The high-purity single crystal with high percentage reactive (001) facets of ant-TiO_2 may cause improved catalytic behaviour and selectivity.[35] Keeping this in view, efforts have been made towards the fabrication of RGO and ant-TiO_2 nanocomposite platform for the fabrication of electrochemical immunosensor. To integrate antTiO_2 with RGO, using a direct self-assembly approach may result in increased *Vander Waal's* interactions between the graphene basal plane and the oxygen moiety present on antTiO_2 surface. A homogeneous distribution of antTiO_2 nanoparticles on multilayered RGO may lead to enhanced electrochemical behavior. Shen *et al*. have synthesized a nancomposite of RGO and TiO_2 nanoparticles.[36] Yun *et al.* have synthesized the RGO–TiO_2 nanotube platform to improve the electron transfer kinetics.[37] Palanisamy *et al.* have fabricated a glucose sensor based on electrodeposition of ZnO microflowers on RGO modified glassy carbon electrode.[38] The low isoelectric point (IEP~ 4.0-5.0) of TiO_2 nanoparticles allows to bind easily with the high IEP of biomolecules especially with the horse reddish peroxides (HRP; IEP~ 8.9). The TiO_2 nanoparticles are known to provide increased stability to HRP molecules. However, direct binding of TiO_2 and HRP labeled antibodies *via* electrostatic interaction may provide a well oriented immune platform that may perhaps preserve the structural integrity of molecules. The favorable orientation of antibodies onto desired surface could be achieved via binding of protein A and G[39] onto the HRP conjugated TiO_2 surface. Li *et al.* have deposited the TiO_2 nanorods on titanium electrode as a supporting matrix for the immobilization of nafion-coated HRP. They have illustrated the strong electrostatic interaction between HRP and TiO_2 nanorods perhaps facilitate direct electron transfer between electrode and biomolecules.[40]

Vibrio cholerae (Vc), is a causative agent for diarrhea, acidosis in humans and is known to cause high lethality.[41] Solanki *et al.* have fabricated nickel oxide nanowires based immunosensor using protein A as a linker for immobilization of anti-*Vibrio cholerea*.[41]A chemiluminescence biosensor has been developed for cholera toxin detection using a supported

lipid membrane as sensing surface and the HRP/ganglioside GM1- functionalized liposome as detection probe.[42]A disposable amperometric immunosensor for *V. cholerae* has been fabricated using the screen-printed electrode of homemade carbon inks consisting of a mixture of polystyrene and graphite particles.[43] Chiriaco *et al.* have developed an electrochemical immunosensor based on mixed self-assembled monolayers of 11-mercaptoundecanoic acid and 2-mercaptoethanol on gold electrode. This electrode can be used to detect cholera toxin from 1-100 ng/mL.[44] Thus, there is an increased demand for the availability of a rapid, sensitive and reproducible analytical tool for the detection of *Vibrio cholerae (Vc)* concentration.

We report results of the studies relating to fabrication of an electrochemical label-free immunosensor for detection of *Vibrio cholerae*. The synthesized TiO_2-RGO composite is electrophoretically deposited onto indium tin oxide (ITO) coated glass substrate for the immobilization of HRP conjugated antibodies-*Vibrio cholerae*. The HRP conjugate antibodies provide a well oriented sensing platform onto TiO_2-RGO nanocomposite resulted in improved sensitivity and a wide detection range. To the best of our knowledge, this is the first time that TiO_2-RGO composite have been used to develop an electrochemical immunosensor for detection of *Vibrio cholerae*.

2. Experimental

2.1 Materials and Reagents

All chemicals have been purchased from Sigma Aldrich, USA. The protein (horse radish peroxidase; HRP) conjugated antibodies specific to *Vibrio cholerae (*Ab-*Vc*), bovine serum albumin (BSA) and *Vibrio cholerae* have been obtained from M/s Genetix Biotech, Asia Pvt. Ltd, India. N-ethyl-N-(3-dimethylaminopropyl) carbodiimide (EDC), N-hydroxysuccinimide (NHS) and graphite powder flakes (45 μm,>99.99 wt%) have been procured from Sigma-Aldrich, USA.

2.2 Synthesis of GO

GO is synthesized using graphite powder flakes *via* improved Hummer's method and purified accordingly to yield a brown powder as described in our previous published work.[24] Briefly, 1.5 gm of graphite powder is pre-oxidized by reacting it with a mixture of 40 mL of 98% H_2SO_4, 5 gm $K_2S_2O_8$ and 5 gm of P_2O_5 for 4 h at 80^oC. The obtained suspension is washed with deionized water for 4-5 times and dried at 50^o C under vacuum. The pre-oxidized graphite is deoxidized by

added a mixture of concentrated H_2SO_4: H_3PO_4 (180: 13) with constant stirring. Then, 9 gm of $KMnO_4$ is added to the mixture after 5 min under continued stirring for 15 h at 50^0C. The reaction is stopped after about 15 h and the reactants are allowed to cool at room temperature after which 200 mL of ice is poured into the mixture followed by 1.5 mL of H_2O_2 (30%). Then fine material separated from the mixture using U.S. standard testing sieve of pore size 30 mm and finally the filtration is performed. The supernatant is discarded and the filtrate is subjected to centrifugation at 5000 rpm for about 3 h. Multiple washing of the sediment material is performed for several times with deionized water, 30% HCl and ethanol (100 mL of each) followed by centrifugation separation. The final sediment is suspended in 100 mL of ether and is filtered through a PTFE membrane with a pore size of 0.45 μm. The semi-solid material obtained as graphene oxide (GO) is vacuum dried overnight. The solid brown powder of GO is thus obtained.

2.3 Reduction of GO

This powder when dispersed in deionized water yields exfoliated sheets of GO upon sonication. The solution is stable over a period of two weeks, without any sign of aggregation. Reduction of GO is performed using the two-step reduction procedure as reported in previous work earlier. [24] On its dispersion in deionized water, the pH of the solution is increased to ~10 using 5 wt % sodium carbonate solution and sodium borohydride ($NaBH_4$) (400 mg) is directly added into 200 mL GO suspension (1 mg/mL) under magnetic stirring and kept at 80^oC for 1h, resulting in a color change from brown to black. The solid product is then purified with water and ethanol washing, followed by drying and re-dispersion in H_2SO_4 at 120 ^{o}C. This is then re-filtered through a 0.22 μm Dura pore membrane to yield RGO. The obtained RGO is partially reduced that consisting of sufficient functional group, controlled by optimized $NaBH_4$ (52 mM) concentration. This chemically active RGO along with the functional group shows good electrochemical properties. Thus, it could be highly valuable for composite formation and attachment of antibodies for development of immunosensor for *Vc* detection.

2.4 Synthesis of ant-TiO_2 nanoparticles

Titanium (IV) butoxide is dissolved in 2-methoxy ethanol to prepare 5(wt%) precursor sol solution via drop wise addition of H_2O and nitric acid under continuously stirred condition to

obtain hydroxide. Further, the anatase titania (ant-TiO_2) has been prepared using a procedure reported earlier.[45]

2.5 Biosensing platform

The RGO and ant-TiO_2 nanocomposite have been fabricated onto ITO (0.25 cm^2) coated glass plate by electrophoretic deposition technique. The interaction between the ant-TiO_2 and RGO occurs electrostatically due to presence of positive charge and negative charge, respectively. A well dispersed stock solution (1:1) of RGO (50 mg/dL) and TiO_2 (50 mg/dL) in acetonitrile is prepared by ultrasonication (50W, 0.25A) for about 3h at room temperature (25^oC). For the fabrication of RGO-ant-TiO_2 nanocomposite 100μL of each stock solution is dispersed in 10mL of acetonitrile to make colloidal suspension of RGO and TiO_2. Electrophoretic deposition is performed in a two-electrode cell by applying DC voltage (100V) for about 2 min. To obtain enhanced deposition, 10^{-5}–10^{-4} mol of $Mg(NO_3)_2.6H_2O$ is added into the suspension that act as electrolyte for EPD that provide net positive charge on the mixture of RGO-ant-TiO_2 that could enhanced the deposition on to anode surface that is ITO. A platinum foil (1cm×2cm) is used as the cathode and a pre-cleaned ITO-coated glass substrate having sheet resistance of 30 Ω cm^{-1} as anode. These two electrodes, separated by 1 cm placed parallel to each other, dipped in the colloidal suspension of RGO-antTiO_2. These RGO-antTiO_2/ITO electrodes are removed from the suspension followed by washing with deionised water and drying.

The zeta potential measurement for RGO-anti TiO_2 composite found that this composite show a net positive charge of +16.8 mV in acetonitrile solvent. Thus, during electrophoretic deposition, the dispersed RGO-anti TiO_2 composite were deposited uniformly on ITO surface under application of negative potential.

Prior to the covalently immobilization of antibodies (Ab-*VC*), the COOH group of the RGO/ITO electrode is activated using EDC as the coupling agent and NHS as activator (Scheme 1). 1ng/mL anti-AFB1 antibody solution is freshly prepared in phosphate buffer (PBS, pH 7.4). Ten microliters of this solution is uniformly spread on the EDC/NHS activated RGO-antTiO_2/ITO electrode surface and is incubated in a humid chamber for about 4 h at room temperature. The covalent interaction can form a strong amide (CO–NH) bond between the carboxyl group of RGO and the amine group of HRP conjugated Ab-*VC*. Moreover, there is possibility to HRP facilitates its naturally electrostatic interactions to antTiO_2 nanoparticles and RGO. This immunoelectrode is rinsed with phosphate buffer (PB; pH 7.0) to remove any

unbound Ab-*Vc*. Finally, Ab-*Vc*/RGO-antTiO$_2$/ITO immunoelectrode is treated with BSA (1 mg/mL) solution for about 4 h to block non-specific sites (Scheme 1). The BSA/Ab-*Vc*/RGO-antTiO$_2$/ITO immunoelectrode is stored at 4°C when not in use.

2.6 Instrumentation

The fabricated RGO-antTiO$_2$/ITO electrode and BSA/Ab-*Vc*/RGO-antTiO$_2$/ITO immunoelectrode have been characterized using Fourier transform infrared spectrometer (FT-IR, PerkinElmer, and Spectrum BX II). X-ray diffraction (XRD) pattern of RGO-antTiO$_2$ film has been obtained via RigakuD/Max 2200 diffractometer with CuK_α radiation at λ=1.5406Å and Raman spectroscopy (HR800 LabRam, Horiba/Jobin-Yvon). Transmission electron microscopy (TEM, Tecnai-G2F30STWINT) and scanning electron microscopy (SEM LEO 440) have been used to investigate the structural and morphological properties of RGO-antTiO$_2$ and BSA/Ab-*Vc*/RGO-antTiO$_2$. The electrochemical analysis has been conducted using an Autolab Potentiostat/Galvanostat with three-electrode system consisting of a working electrode, platinum wire as auxiliary electrode, and Ag/AgCl act as reference electrode in phosphate buffer saline (PBS, pH 7.0, 0.9% NaCl) containing 5 mM$[Fe(CN)_6]^{3-/4-}$ as redox probe.

3. Results and Discussions

3.1 X-ray diffraction studies

Figure 1 shows XRD pattern of RGO (a) and antTiO$_2$-RGO (b). The broad and dominating peak seen at 24^o (3.43A^o) corresponds to (002) reflection plane indicating reduction of the GO due to removal of the intercalated water molecules and the oxide groups of GO that allow RGO sheet to pack tighter (smaller interlayer distance between sheets).[36]The RGO-antTiO$_2$ nanohybrid shows a prominent peak at 2θ: 25^o and 48^o, corresponding to diffraction from (101) and (200) planes indicating anatase phase of TiO$_2$. The other diffraction planes observed for (004),(105),(211),(204)(JCPDS 894921) reveal the presence of anatase phase in TiO$_2$. The TiO$_2$ naoparticles show all the peaks relating to ant-TiO$_2$ (Supplementary data S1). However, in the RGO-antTiO$_2$ composite, the diffraction plane (200) shows a weak peak corresponding to (101), indicating that the observed RGO layers are separated by nanoparticles via spacers and are not stacked together).[46] The average crystallite size of the antTiO$_2$ nanoparticles is estimated to be about 12nm based on Scherrer's equation. No clear diffraction peak pertaining to graphite is observed, suggesting that the graphene sheet has a disordered structure.

3.2 Transmission electron microscopy (TEM) studies

Figure 2A and B shows results of the TEM studies conducted for synthesized nanostructured TiO_2 and RGO-antTiO_2 hybrid. The collidal solutions of TiO_2 and RGO-antTiO_2 composite have been prepared on carbon coated copper grid by electrophoretic technique. Image (A) shows the anatase TiO_2 nanoparticles which are uniformly distributed. Some of the nanoparticles are agglomerated due to surface charge among the nanoparticles. The average size of the TiO_2 nanoparticles varies from 10 to 15 nm and is in agreement with the results of XRD studies. It appears that RGO has a crumpled layered structure with several stacking layers of the monoatomic graphene sheets (image 2B). The TEM image shows edges of graphene sheets attached with spherical shaped TiO_2 nanoparticles on its surface indicating anchoring of TiO_2 nanoparticles on graphene sheets. And at edges of the graphene sheet, TiO_2 nanoparticles agglomerate due to the presence of TiO_2 nanoparticles.

3.3 Scanning electron microscopic studies

Figure 2 (C and D) shows results of the scanning electron microscopic studies observed before and after immobilization antibodies on RGO-antTiO_2 composite. The image C shows that the titania nanoparticles wrapped with graphene nanosheets can be seen on a larger graphene flakes (highlighted by red circle). In addition, some of these sheets are folded on the edges and in some region wrinkles can be clearly seen. While after antibody attachment (image D) the fine thread like structure appears all over the RGO flakes indicating antibody molecules (immobilized antibody molecules are highlighted by yellowed dashed arrows and circle). However, the image D shows the smooth surface indicating that the RGO-antTiO_2 nanohybrid surface is covered by the immobilized antibodies and BSA *via* π- π interactions.

3.4 Atomic Force Microscopic Studies

Figure 2 (E and F) shows the two-dimensional atomic force microscopy (AFM) image of prepared bare rGO film. Micron size rGO flakes are distributed on ITO substrate. The distribution height profile is shown below of the image (E). Some of the rGO sheets attached each other due to π-π stacking resulting in bigger size of sheets. After TiO_2 functionalization, the roughness of the rGO film is increased (image F) to 0.137 micron compared to bare rGO (roughness: 76.4 nm). The TiO_2 nanoparticles are attached on rGO sheets on basal plane as well as edges during its deposition on ITO that enhance roughness of the film.

3.5 Raman spectroscopy studies

Raman spectroscopy studies have been carried out to confirm the synthesis of RGO and RGO-antTiO$_2$ nanohybrid [Fig. 3A]. The inset shows absorption peak at 1348 cm^{-1} indicating D band arising due to the carbon atoms vibrations with sp^3 electronic configuration of disordered graphene. The peak at 1589 cm^{-1} pertaining to the G band is associated with in-plane vibration of the sp^2-bonded carbon atoms. The Raman spectrum of RGO-antTiO$_2$ shows peaks in the low frequency region pertaining to the B1g (399 cm^{-1}), A1g (513 cm^{-1}) and Eg (637 cm^{-1}) mode of the anatase phase. The intensity of D band (1348 cm^{-1}) is found to be decreased as compared to that of the RGO (inset). And the wavenumber is slightly shifted towards the lower side indicating the formation of RGO-antTiO$_2$ nanohybrid. The intensity ratio of D/G of antTiO$_2$–RGO is found to be low (0.95) as compared to that of RGO (1.28) due to increased average size of the sp^2 domain and defects in RGO. In case of the GO sheet, a decreased D/G intensity ratio is observed, suggesting that the defects in graphene sheet increase after the reduction of GO.

3.6 Fourier transform infrared spectroscopy and UV-Vis studies

FT-IR spectra of RGO-antTiO$_2$/ITO film show the absorption peak at 579 cm^{-1} (Ti-O bond) (Supplementary data, Fig.S2). The peak seen at 961cm^{-1} corresponds to C-H stretching vibration on nanocomposite surface. Absorption peaks at 1052 cm^{-1} and 1225 cm^{-1}(C–O stretching vibration), 1664 cm^{-1}(C=C aromatic) 1746 cm^{-1} (C=O stretching vibration of COOH groups) indicate the presence of GO sheets in the RGO-antTiO$_2$/ITO film. The intense peak found near 1600 cm^{-1} arises due to vibrations from the un-oxidized graphitic domains. The intensity of absorption peak at 1600 cm^{-1} increases due to amide bond formation after immobilization of Ab-*Vc* and BSA (curve b). The peak shift in the finger print region (500-600 cm^{-1}) arises due to incorporation of Ab-*Vc* followed by BSA onto RGO-antTiO$_2$/ITO nanohybrid surface. The additional peaks seen at 1047 cm^{-1}, 2030 cm^{-1}, 3200 cm^{-1} (curve b) reveal surface functionalization with Ab-*Vc* and BSA.

The UV-Vis studies have been conducted on antTiO$_2$ (i), RGO-antTiO$_2$ (ii) and Ab-*Vc*/RGO-antTiO$_2$ (iii) electrodes in the wavelength range, 200 to 700 nm (Supplementary data, Fig. S3). The absorption peak found at 265 nm is due to quantum confinement effect of the antTiO$_2$. The direct band gap has been determined where $(\alpha h\upsilon)^2$ plots verses energy band plot (Fig. 3(ii)) using Tauc equation

$$(\alpha h\upsilon)^2 = k(h\upsilon - E_g) \qquad \text{Eq. (1)}$$

where α is the absorbance, h is Plank constant and k is a constant. The direct band gap (E_g) of antTiO_2 [Fig. 3 (B),(a)] has been estimated to be 3.8 eV which is higher compared to that of the bulk material. It can be seen that the distinct peaks appear at 334 nm and 250 nm corresponding to π-π* transition of aromatic C-C bond of RGO modified antTiO_2. The band gap of antTiO_2 electrode decreases to 2.55 eV due to incorporation of RGO [curve (b)]. The intensity of the peak is found to be enhanced after the conjugation of antibodies with RGO-antTiO_2 indicating binding of the antibodies confirms the binding of antibodies onto nanocomposite surface. The band gap of Ab-*Vc*/RGO-antTiO_2 has been found as 2.68 eV [curve (c)].

3.7 Cyclic voltammetry studies

The cyclic voltammetry (CV) studies of the bare ITO electrode (a), RGO-antTiO_2/ITO nanohybrid (b), Ab-*Vc*/RGO-antTiO_2/ITO immunoelectrode (c) and BSA/Ab-*Vc*/RGO-antTiO_2/ITO immunoelectrode (d) have been performed in PBS containing 5 mM$[Fe(CN)_6]^{3-/4-}$ at scan rate of 20 mV/s (Supplementary data, Fig.S4). It can be seen that magnitude of current of RGO-antTiO_2/ITO electrode increases by about 4-fold (4.44 μA; curve b) and the oxidation current shifts toward the higher potential compared to that of the bare ITO (1.46 μA; curve a) due to fast electron transfer between the electrode and electrolyte. This may be attributed to the heterogeneous electron transfer in graphene sheet and oxygen-containing groups at the edges of the graphene sheets. Besides this, the excellent electrocatalytic ant-TiO_2 embedded into the RGO results in faster electron communication between the electrode and electrolyte. The RGO-antTiO_2/ITO electrode has been functionalized with a macromolecular proteins conjugated Ab-*Vc* leading to decreased flow of electrons resulting in reduced current (4.09 μA; curve c) with slight shift towards lower potential due to insulating nature of protein molecules (HRP labeled Ab-*Vc)*. The modification of the Ab-*Vc*/RGO-antTiO_2/ITO electrode with the insulating BSA (used as a blocking agent for the non binding sites) results in hindered electron transfer between medium and electrode leading to decrease in magnitude of the current.

The cyclic voltammetric studies of the RGO-antTiO_2/ITO nanohybrid and BSA/Ab-*Vc*/ RGO-antTiO_2/ITO immunoelectrode have been carried out as a function of scan rate (10-100 mV/s) [Fig. 4 (A)]. It has been observed that magnitude of the redox current proportionally increases (I_a is anodic) with respect to square root of scan rate indicating the diffusion-controlled system [inset: Fig.4 (A)]. The variation of current for different electrodes follows Eq.2 to 5.

$$I_{pa}(A)_{\mathrm{RGO-antTiO_2\ nanohybride}} = 3.38 \times 10^{-6}A + 6.57 \times 10^{-5}A\ (s/V) \times scan\ rate\ (V/s)\ with\ R^2 = 0.989 \ldots (2)$$

$$I_{pc}(A)_{\mathrm{RGO-antTiO_2\ nanohybride}} = -3.34 \times 10^{-6}A - 4.14 \times 10^{-5}A\ (s/V) \times scan\ rate\ (V/s)\ with\ R^2 = 0.99 \ldots . (3)$$

$$I_{pa}(A)_{BSA/Ab-Vc/\mathrm{RGO-antTiO_2\ immunoelectrode}} = 1.42 \times 10^{-6}A + 3.62 \times 10^{-5}A\ (s/V) \times scan\ rate\ (V/s)\ with\ R^2 = 0.99 . . (4)$$

$$I_{pc}(A)_{BSA/Ab-Vc/\mathrm{RGO-antTiO_2\ immunoelectrode}} = -1.31 \times 10^{-6}A - 1.02 \times 10^{-5}A\ (s/V) \times scan\ rate\ (V/s)\ with\ R^2 = 0.965 \ldots (5)$$

The surface concentration of RGO-antTiO$_2$/ITO nanohybrid and BSA/Ab-*Vc*/RGO-antTiO$_2$/ITO immunoelectrode has been estimated from the plot of current verses potential (CV) using equation: $I_p = \frac{n^2F^2I^*AV}{4RT}$ (Brown–Anson model), where *n* is the number of electrons transferred, *F* is the Faraday constant (96,584 C/mol), *I** is the surface concentration (mol/m^2), *A* is surface area of the electrode (0.25×10^{-4} m^2), *V* is the scan rate (0.02 V/s), *R* is gas constant [8.314 J/(mol K)], and *T* is absolute temperature (298 K). The surface concentration for RGO-antTiO$_2$/ITO nanohybrid and BSA/Ab-*Vc*/RGO-antTiO$_2$/ITO immunoelectrode has been found as 23.7 and 15.4mol/m^2, respectively. The change in surface concentration reveals the immobilization of antibodies onto RGO-antTiO$_2$/ITO electrode.

3.8 Impedance studies

The electrochemical impedance spectroscopy (EIS) involves application of a sinusoidal ac potential, $E_t=E_0\sin(\omega t)$ and $\omega = \pi f$ with dc offset potential.[47] In a linear system, the response signal (I_t), is shifted in phase (φ) and has a different amplitude, I_0, where $I_t = I_0 \sin(\omega t + \varphi)$. Fourier transform of the voltage and current ratio gives the impedance response over a frequency range, given by Eq. 6

$$Z = \frac{E_t}{I_t} \quad (6)$$

The constant phase element (CPE) represents capacitance between the electrode and electrolyte and its impedance value is given by following equation.

$$Z_{CPE} = \frac{1}{Y_0(j\omega)^{\alpha}};\quad \alpha = \frac{\Phi}{90} \quad (7)$$

where, Y_0 represents the capacitance (CPE) and $j=\sqrt{-1}$. The average capacitance for the CPE Helmhotz (a) and CPE Randles (b) equivalent circuit (Supplementary data; Scheme A) are given by Barsoukov et al., 2005[48] as in Eq.(8) and (9), respectively. The magnitude of capacitance can be estimated using the equivalent circuit model by fitting.

$$C = \sqrt[\alpha]{\frac{Y_0}{R_{soln}^{-1}}} \quad (8)$$

$$C = \sqrt[\alpha]{\frac{Y_0}{R_{immunoelctrode}^{-1} + R_{soln}^{-1}}} \quad (9)$$

The CPE value of RGO-antTiO$_2$/ITO nanohybrid (a), Ab-*Vc*/RGO-antTiO$_2$/ITO immunoelectrode (b) and BSA/Ab-*Vc*/RGO-antTiO$_2$/ITO immunoelectrode (c) has been found to be as 1.72×10^{-6} F, 0.67×10^{-6} F and 0.28×10^{-6}F, respectively [Fig. 4 B]. It has been observed that the constant phase element decreases after incorporation of Ab-*Vc* and BSA onto RGO-antTiO$_2$/ITO nanohybrid based electrode. This is perhaps due to increased double layer distance between the BSA/Ab-*Vc*/RGO-antTiO$_2$/ITO immunoelectrode and electrolyte.

The semicircle diameter obtained from the EIS spectra from Randles equivalent circuit is the charge transfer resistance (R_p). The charge transfer resistance controls the electron transfer kinetics of the redox-probe at electrode/electrolyte interface. The change in the Rp value due to addition of different substances adsorbed onto the electrode surface indicates surface modification. In this context, the Nyquist plots of Randles equivalent circuit i.e. Z_{im} as a function of Z_{re}, with frequency range, $0.01–10^5$ Hz has been obtained for bare ITO electrode (a), RGO-antTiO$_2$/ITO nanohybrid (b), Ab-*Vc*/RGO-antTiO$_2$/ITO immunoelectrode (c) and BSA/Ab-*Vc*/RGO-antTiO$_2$/ITO immunoelectrode (d), respectively [Fig. 4 B]. The linear fit of the RGO-antTiO$_2$/ITO electrode exhibits nearly straight line resulting in increased diffusion compared to that of the bare ITO (curve a). This may be due to presence of increased concentration of defects at the RGO-antTiO$_2$ nanohybrid that perhaps inhibits direct electron flow from the redox probe$[Fe(CN)_6]^{3-/4-}$ to the electrode surface. However, after the immobilization of Ab-*Vc* and BSA onto RGO-antTiO$_2$/ITO surface, the diffusion of electrons between the electrode and the redox ions decreases resulting in increase in R_p value (2.28 kΩ, 2.89 kΩ; curve c & d). This may be assigned to the presence of bulky protein molecules that provide steric hindrance. In addition, the electrostatic interaction between the Ab-*Vc* and BSA and redox ions, or a change in the electronic properties of RGO-antTiO$_2$/ITO nanohybrid may result in reduced value of R_p. However, increased value of R_p, indicates superior electrochemical reactivity of Ab-*Vc*/RGO-antTiO$_2$/ITO immunoelectrode. The relative change in R_p for the Ab-*Vc*/RGO-antTiO$_2$/ITO immunoelectrode and quantifies the R antibody molecules. R_p^0 is the charge transfer after interaction of CT with the Ab-*Vc*/RGO-antTiO$_2$/ITO immunoelectrode.

$$\Delta R_p = \frac{(R_p - R_p^0)}{R_p^0} \qquad (10)$$

Table 1 shows values of the impedance obtained for different circuit elements used in modeling the sensor.

3.9 Electrochemical response studies

The impedimetric response of BSA/Ab-*Vc*/RGO-antTiO$_2$/ITO immunoelectrode has been measured as a function of *Vibrio cholerae* concentration varying from 10 to 450ng/mL in PBS containing $[Fe(CN)_6]^{3-/4-}$ with incubation time of about five minutes [Fig.5 A]. It has been found that the capacitance decreases with increased *Vc* concentration. It may perhaps be assigned to the antibody-antigen (Ab-Ag) interaction leading to change in dielectric/blocking properties of the electrolyte-electrode interface.[49-50] The capacitance value between the RGO-antTiO$_2$ based immunoelectrode and the electrolyte is $\frac{\varepsilon\varepsilon_o \mathrm{A}}{d}$, where $\boldsymbol{\varepsilon}_0$(Fm^{-1}) is the permittivity of free space, $\boldsymbol{\varepsilon}$ is the relative dielectric constant, A(m^2) is the surface area and d(m) is the distance. The decrease of the measured capacitance due to the increase of the distance between the electrode and electrolyte is thus expected due to interaction of the *Vc* to Ab-*Vc*. In addition, the interaction between Ab-*Vc* and *Vc* causes decrease in the magnitude of capacitance since less polar protein (*Vc*) molecules replace water molecules from the electrode surface. The capacitive immunosensor can be calibrated by plotting change in the capacitance versus the analyte (antigen) concentration. This calibration curve exhibits a linear fit as $C_{dl}(F) = 0.64 \times 10^{-6}\,(F) + 4.52 \times 10^{2} F/\,\mathrm{mol\,l^{-1}} \times \{Vc\ \mathrm{concentartion}\}$. A linear relationship is observed in the range, 10-450 ng/mL (0.12-5.4 nmol l^{-1}). The change in the capacitance (R_p) value of BSA/Ab-*Vc*/RGO-antTiO$_2$/ITO immunoelectrode has been monitored as a function of *Vc* under similar conditions [Fig.5 A]. It has been found that the R_p value increases on addition of *Vc* concentration on the BSA/Ab-*Vc*/RGO-antTiO$_2$/ITO immunoelectrode [Fig. 5 B]. This is due to the antigen-antibody complex formation of *Vc* at the electrode surface. The increased R_p value indicates that the insulating layer of BSA/Ab-*Vc*/RGO-antTiO$_2$/ITO immunoelectrode surface inhibits penetration of the redox species to the electrode surface resulting in higher diameter of EIS spectra. The linear relationship has been observed between the value of capacitance of the BSA/Ab-*Vc*/RGO-antTiO$_2$/ITO immunoelectrode and *Vc* concentration [Fig.5 A]. The charge transfer resistance (R_{ct}) of the BSA/Ab-*Vc*/RGO-antTiO$_2$/ITO immunoelectrode and *Vc* concentration has been found to increase with increasing concentrations of *Vc* [inset, Fig. 5 B]. The immunoelectrode when treated with the 0.2 M glycine solution of pH 2.4 for about two minutes results in 95% of the regenerated immunoelectrode.

The kinetics of this immunosensor has been investigated using EIS at room temperature (298 K). The binding reaction equation between the antigen and antibodies has been calculated

as$[A] + [B] \leftrightarrow [AB]$. The rate of formation of complex between antigen and antibodies as the association phase as given in following equation (11).

$$\frac{d[AB]}{dt} = k_a [A][B] - k_d [AB] \quad \text{(Eq. 11)}$$

where, k_a and k_d are the association and dissociation rate constants, respectively. The association and dissociation rate constants for Ab-*Vc* binding are estimated to be as 5.845 ng/mL(0.07 nM) and 0.171 ng/mL(0.002 nM), respectively. The equilibrium constant for association ($K_A = k_a/k_d$) is found as 34.18 ng/mL(0.41 nM). These results indicate that the strong binding affinity of the BSA/Ab-*Vc*/RGO-antTiO_2/ITO immunoelectrode with a *Vibrio cholerae* moiety. The change in electrochemical response studies of BSA/Ab-*Vc*/RGO-antTiO_2/ITO immunoelectrode as a function of *Vibrio cholerae* [10-450 ng/mL] has been investigated using CV at similar condition. The magnitude of peak current decreases as the concentration of *Vibrio cholerae* increases [Fig. 5 (C)]. This may due to antigen-antibody interaction on transducer surface which blocks the charge transfer from electrolyte to electrode. The transfer of electrons from $[Fe(CN)_6]^{3-/4-}$ redox conversation may blocked due to formation of highly organized layers on the electrode surface because these redox species do not penetrate the layer and enter into the conductive electrode surface. Addition of *Vc* moiety on BSA/Ab-*Vc*/RGO-antTiO_2/ITO immunoelectrode, this protein molecules (*Vc*) formed an insulating layer formed on the electrode results in increased diameter of the semicircle, implying higher charge transfer resistance. The detection range obtained from 10-450 ng/mL with sensitivity 1.6 μA ng mL^{-1}/cm^2 and linear regression coefficient (r^2) of 0.99. The electrochemical response studied has been conducted on without incorporating TiO_2 nanoparticles on RGO bioelectrode as function of *Vc* concentration (Fig. S5). It has been found that the detection range as 100-300 ng/mL and sensitivity 0.22 μA/ng mL^{-1} with r^2 of 0.92 which is less than the BSA/Ab-*Vc*/RGO-antTiO_2/ITO immunoelectrode.

The BSA/Ab-*Vc*/RGO-antTiO_2/ITO immunosensor yields high sensitivity 21.8×10^{-3} μF/ng mL^{-1}/cm^2 (18.17×10^6 F/mol l^{-1}/m^2) with standard deviation of 2.556 and a linear regression coefficient (r^2) of 0.986. The higher sensitivity of this fabricated biosensor may be due to the functional property and larger surface area of RGO-antTiO_2 nanohybrid. The presence of available functional groups on RGO-antTiO_2 may increase the loading capacity of antibody molecules resulting in improve biosensor efficacy. This immunosensor shows a lower detection value as 0.148 ng/mL (0.0018 nmol l^{-1}) calculated using the $3\sigma_b/m$ criteria, where m is slope of

the calibration graph and σ_b is the standard deviation of the blank signal. The wide detection range of *Vc* obtained as [10-450 ng/mL][0.12-5.4 nmol l^{-1}]. Solanki *et al.* have reported nickel oxide nanowire-based electrochemical biosensor for detection of *Vc* concentration [37–350 ng/mL][0.44-4.2 nmol l^{-1}].[41] Thus, compared to individual metal oxide, nanohybrid metal oxide/graphene composite is a potential candidate for fabrication of biosensor to detect *Vc* concentration.

3.9 Specificity reproducibility and stability tests

The specificity of immunoelectrode (BSA/Ab-*Vc*/RGO-antTiO_2/ITO) has been tested against glucose (5mM), uric acid (5mM), *Escherichia coli* (300 ng/mL) and *Salmonella typhi* (300 ng/mL) and *Vibrio cholerae* (300 ng/mL). This immunoelectrode has been incubated (5 min) by adding of 15 µl of these metabolites and pathogens. During these measurements, it is observed that there are no significant changes in electrochemical response after interaction of the pathogens with BSA/Ab-*Vc*/RGO-antTiO_2/ITO immunoelectrode [Fig. S6]. Thus, indicating specificity of the probe for *Vibrio cholera.*

The reproducibility of the immunoelectrode (BSA/Ab-*Vc*/RGO-antTiO_2/ITO) has been investigated at 300 ng/mL of *Vibrio cholerae* concentration with different electrode and change in magnitude of current is observed. It has been observed that no significant change in current value indicating good precision [Fig. S7]. The storage stability of immunoelectrode has been monitored by recording CV at different time interval of 10 days for about 50 days [Fig. S8]. It has been observed that no significant current change occurs up to 50 days after which 5 % change in current is observed compared to the original value. Thus, BSA/Ab-*Vc*/RGO-antTiO_2/ITO immunoelectrode reveals excellent storage stability upto 50 days.

4. Conclusions

We have demonstrated the fabrication of a label-free immunosensor based on RGO-antTiO_2 nanohybrid for detection of *Vibrio cholerae*. The RGO-antTiO_2 nanohybrid platform has been utilized for loading of protein conjugated antibodies specific to *Vibrio cholerae* (Ab-*Vc*). The capacitive property of this RGO-antTiO_2 nanohybrid smart material is explored to detect *Vibrio cholerae* based on their antigen-antibody interactions. Electron microscopy, XRD and UV studies reveal successful formation of RGO-antTiO_2 nanohybrid material whereas FT-IR and electrochemical investigations suggest its functionalized nature that is desired for antibody attachment. The electrochemical response studies of the BSA/Ab-*Vc*/RGO-antTiO_2/ITO

immunoelectrode as a function of *Vibrio cholerae* concentration reveals higher sensitivity, improved low detection limit (10ng mL^{-1})(0.12 nmol l^{-1}) and long term stability (50 days) arising due to excellent electrochemical properties and high electron transfer kinetics of RGO-antTiO_2. The results indicate that RGO-antTiO_2 is an interesting platform for the immobilization of *Ab-Vc*. The superior sensing (supercapacitive) performance of the RGO-antTiO_2 based immunosensor reveals its potential application in medical diagnostics. This technique provides the opportunity to achieve effective determination of *Vc* using miniaturized devices based on RGO-antTiO_2 nanohybrid material and could be a better choice for clinical diagnostics.

Acknowledgements

PRS is grateful to the Department of Science and Technology (DST), India for Young Scientist Award and other financial support. Saurabh Srivastava and Md. Azahar Ali thank CSIR for award of Senior Research Fellowships.

References:

1. A. P. F. Turner, *Chem. Soc. Rev.*, 2013, **42**, 3184.
2. M. A. Ali, S. Srivastava, P. R. Solanki, V. Reddy, V. V. Agrawal, C. Kim, R. John and B. D. Malhotra, *Sci. Reports*, 2013, **3**, 2661.
3. P. R. Solanki, A. Kaushik, V. V. Agrawal and B. D. Malhotra, *NPG Asia Mater.*, 2011, **3**, 17.
4. D. Zhai, B. Liu, Y. Shi, L. Pan, Y. Wang, W. Li, R. Zhang and G. Yu, *ACS Nano*, 2013, **7**, 3540.
5. N. Gilmartin and R. O'Kennedy, *Enzyme and Microbial Technology*, 2012, **50**, 87.
6. P. C. Ray, S. A. Khan, A. K. Singh, D. Senapati and Z. Fan, *Chem. Soc.Rev.*, 2012, **41**, 3193.
7. T. Kuila, S. Bose, P. Khanra, A. K. Mishra, N. H. Kim and J. H. Lee, *Biosens. Bioelectron.*, 2011, **26**, 4637.
8. P. R. Solanki, M. K. Patel, A. Kaushik, M. Pandey, R. Kotnala and B. Malhotra, *Electroanalysis*, 2011, **23**, 2699.
9. Y. Yang, A. M. Asiri, Z. Tang, D. Du and Y. Lin, *Mater. Today*, 2013, **16**, 365.
10. Y.C. Chen, X.C. Huang, Y.L. Luo, Y.C. Chang, Y.Z. Hsieh and H.Y. Hsu, *Sci.Tech. Advan.Mater.*, 2013, **14**, 044407.

11. V. Biju, *Chem. Soc. Rev.*, 2014, **43**, 744.
12. W. Yang, K. R. Ratinac, S. P. Ringer, P. Thordarson, J. J. Gooding and F. Braet, *Angewandte Chemie International Edition*, 2010, **49**, 2114.
13. Y. Shao, J. Wang, H. Wu, J. Liu, I. A. Aksay and Y. Lin, *Electroanalysis*, 2010, **22**, 1027.
14. L. Zhang, Y. Li, L. Zhang, D.W. Li, D. Karpuzov and Y.T. Long, *Int. J. Electrochem. Sci*, 2011, **6**, 819.
15. A. Galal, N. F. Atta and H. K. Hassan, *Int. J. Electrochem. Sci*, 2012, **7**, 768.
16. G. Eda, G. Fanchini and M. Chhowalla, *Nature Nanotech.*, 2008, **3**, 270.
17. C. S. Rout, P. D. Joshi, R. V. Kashid, D. S. Joag, M. A. More, A. J. Simbeck, M. Washington, S. K. Nayak and D. J. Late, *Sci. Reports*, 2013, **3**.
18. A.M. J. Haque, H. Park, D. Sung, S. Jon, S.Y. Choi and K. Kim, *Anal.Chem.*, 2012, **84**, 1871.
19. M. Zhou, Y. Zhai and S. Dong, *Anal. Chem.*, 2009, **81**, 5603.
20. J. D. Fowler, M. J. Allen, V. C. Tung, Y. Yang, R. B. Kaner and B. H. Weiller, *ACS Nano*, 2009, **3**, 301.
21. S. Liu and X. Guo, *NPG Asia Mater.*, 2012, **4**, e23.
22. Z. Yin, S. Sun, T. Salim, S. Wu, X. Huang, Q. He, Y. M. Lam and H. Zhang, *ACS nano*, 2010, **4**, 5263.
23. B. Chitara, L. Panchakarla, S. Krupanidhi and C. Rao, *Advan. Mater.*, 2011, **23**, 5419.
24. S. Srivastava, V. Kumar, M. A. Ali, P. R. Solanki, A. Srivastava, G. Sumana, P. S. Saxena, A. G. Joshi and B. Malhotra, *Nanoscale*, 2013, **5**, 3043.
25. S. Bai and X. Shen, *RSC Advances*, 2012, **2**, 64.
26. P. Wang, Y. Zhai, D. Wang and S. Dong, *Nanoscale*, 2011, **3**, 1640.
27. K. Gotoh, T. Kinumoto, E. Fujii, A. Yamamoto, H. Hashimoto, T. Ohkubo, A. Itadani, Y. Kuroda and H. Ishida, *Carbon*, 2011, **49**, 1118.
28. S. Guo and S. Dong, *Chem. Soc. Rev.*, 2011, **40**, 2644.
29. Z. S. Wu, D. W. Wang, W. Ren, J. Zhao, G. Zhou, F. Li and H. M. Cheng, *Advan. Funct. Mater.*, 2010, **20**, 3595.
30. Y. Wang, Z. Li, J. Wang, J. Li and Y. Lin, *Trends in Biotech.*, 2011, **29**, 205.
31. Y. Zou and Y. Wang, *Nanoscale*, 2011, **3**, 2615.

32. Z.S. Wu, G. Zhou, L.C. Yin, W. Ren, F. Li and H.M. Cheng, *Nano Energy*, 2012, **1**, 107.
33. S. Zhu, J. Guo, J. Dong, Z. Cui, T. Lu, C. Zhu, D. Zhang and J. Ma, *Ultrasonics Sonochem.*, 2013, **20**, 872.
34. P. Wang, Y. Tang, Z. Dong, Z. Chen and T.T. Lim, *J. Mater. Chem. A*, 2013, **1**, 4718.
35. X.Y. Zhang, H.P. Li, X.L. Cui and Y. Lin, *J.Mater. Chem.*, 2010, **20**, 2801.
36. J. Shen, M. Shi, B. Yan, H. Ma, N. Li and M. Ye, *Nano Research*, 2011, **4**, 795.
37. J.H. Yun, R. J. Wong, Y. H. Ng, A. Du and R. Amal, *RSC Advances*, 2012, **2**, 8164.
38. S. Palanisamy, S. Cheemalapati and S.M. Chen, *Int J Electrochem.Sci.*, 2012, **7**, 8394.
39. S. Boujday, A. Bantegnie, E. Briand, P.G. Marnet, M. Salmain and C.M. Pradier, *J. Phys. Chem.B*, 2008, **112**, 6708.
40. Q. Li, K. Cheng, W. Weng, P. Du and G. Han, *Microchim. Acta*, 2013, **180**, 1487.
41. P. R. Solanki, M. A. Ali, V. V. Agrawal, A. Srivastava, R. Kotnala and B. Malhotra, *RSC Advances*, 2013, **3**, 16060.
42. H. Chen, Y. Zheng, J.-H. Jiang, H.L. Wu, G.L. Shen and R.Q. Yu, *Biosens. Bioelectron.*, 2008, **24,** 684.
43. V. K. Rao, M. K. Sharma, A. K. Goel, L. Singh and K. Sekhar, *Anal Sci*., 2006, **22**,1207.
44. M. Serenaa Chiriac and R. ElenaáIonescu, *Lab Chip*, 2011, **11**, 658.
45. M. A. Ali, S. Srivastava, P. R. Solanki, V. V. Agrawal, R. John and B. D. Malhotra, *Appl. Phys. Lett.*, 2012, **101**, 084105.
46. C. Nethravathi and M. Rajamathi, *Carbon*, 2008, **46**, 1994.
47. G. K. Lewis Jr, G. K. Lewis Sr and W. Olbricht, *Measurement Science and Technology*, 2008, **19**, 105102.
48. E. Barsoukov and J.R.Macdonald, 2005. Impedance Spectroscopy; Theory, Experiment, and Applications, 2nd ed., Wiley Interscience Publications.
49. P. Bataillard, F. Gardies, N. Jaffrezic-Renault, C. Martelet, B. Colin and B. Mandrand, *Anal.Chem.*, 1988, **60**, 2374.
50. I. O. K'Owino and O. A. Sadik, *Electroanalysis*, 2005, **17**, 2101.

Figure Captions

Scheme 1. Fabrication of immunosensor for *Vibrio cholerae* detection

Figure 1. Powder X-ray diffraction pattern of RGO (a) and RGO-antTiO_2 (b)

Figure 2 (A) TEM of TiO_2 nanoparticles; (B) RGO-antTiO_2 composite; (C) and (D) SEM images of RGO-antTiO_2 composite and BSA/Ab-*Vc*/RGO-antTiO_2/ITO bioelectrode, respectively. And AFM images (E) and (F) of RGO/ITO electrode and RGO-antTiO_2/ITO, respectively

Figure 3 (A) Raman spectra of RGO-antTiO_2 nanohybrid and Raman spectra of RGO (inset) and (B) curve between $(\alpha h\upsilon)^2$ verses energy band (eV) plots.

Figure 4 (A) CV spectra of RGO-antTiO_2/ITO nanohybrid at different scan rate various from 10-100 mV/s. (B) EIS of bare ITO electrode (a), RGO-antTiO_2/ITO nanohybrid (b), Ab-*Vc*/RGO-antTiO_2/ITO immunoelectrode (c) and BSA/Ab-*Vc*/RGO-antTiO_2/ITO bioelectrode (d).

Figure 5 (A) Electrochemical impedance response studies of BSA/Ab-*Vc*/RGO-antTiO_2/ITO immunoelectrode as a function of *Vibrio cholerae* concentration [10-450 ng/ml]

Figure 5 (B) Calibration plot between capacitance of the BSA/Ab-*Vc*/RGO-antTiO_2/ITO immunoelectrode and *Vibrio cholerae* concentration (inset: Calibration plot between charge transfer resistance (R_{ct}) of the BSA/Ab-*Vc*/RGO-antTiO_2/ITO immunoelectrode and *Vibrio cholerae* concentration).

Figure 5 (C) The response studies of BSA/Ab-*Vc*/RGO-antTiO_2/ITO immunoelectrode as function of *Vibrio cholerae* concentration. Inset shows the plot between the current value verses *Vibrio cholerae* concentration.

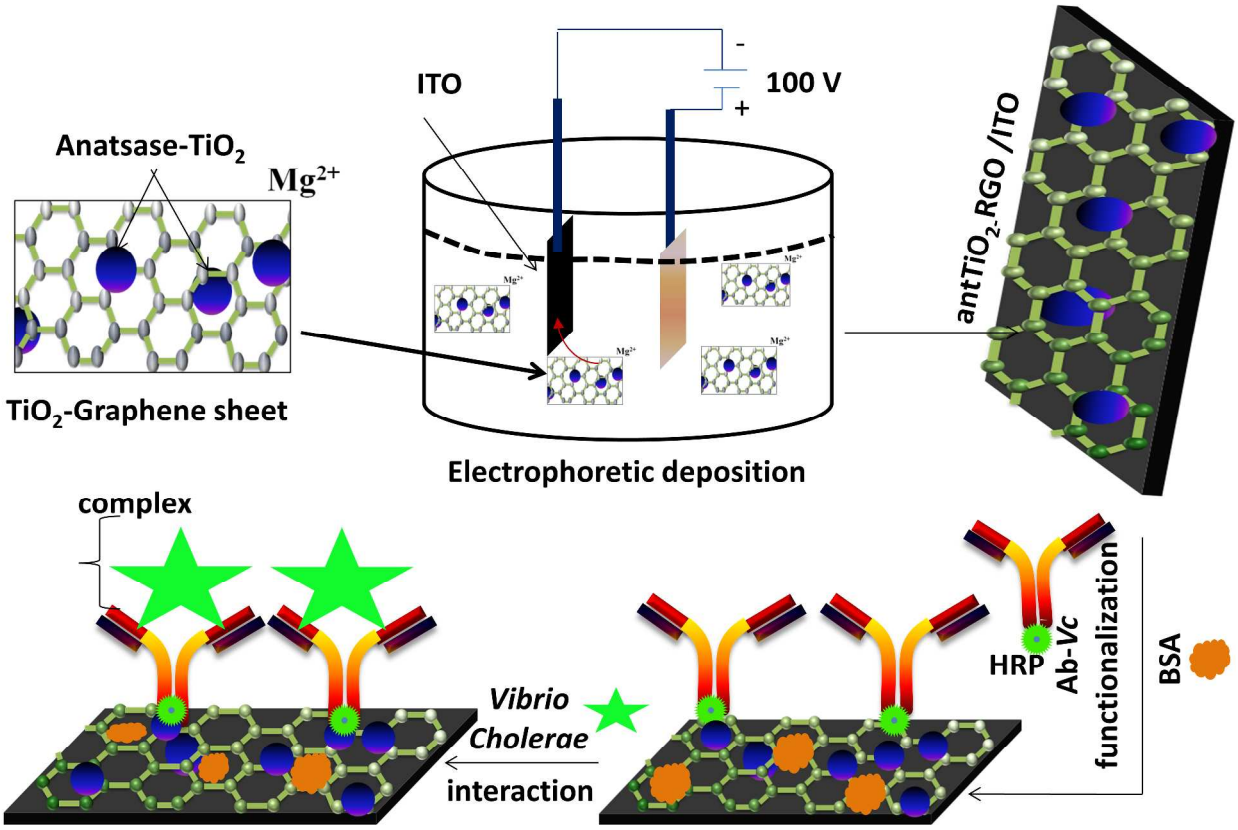

Scheme 1

Figure 1

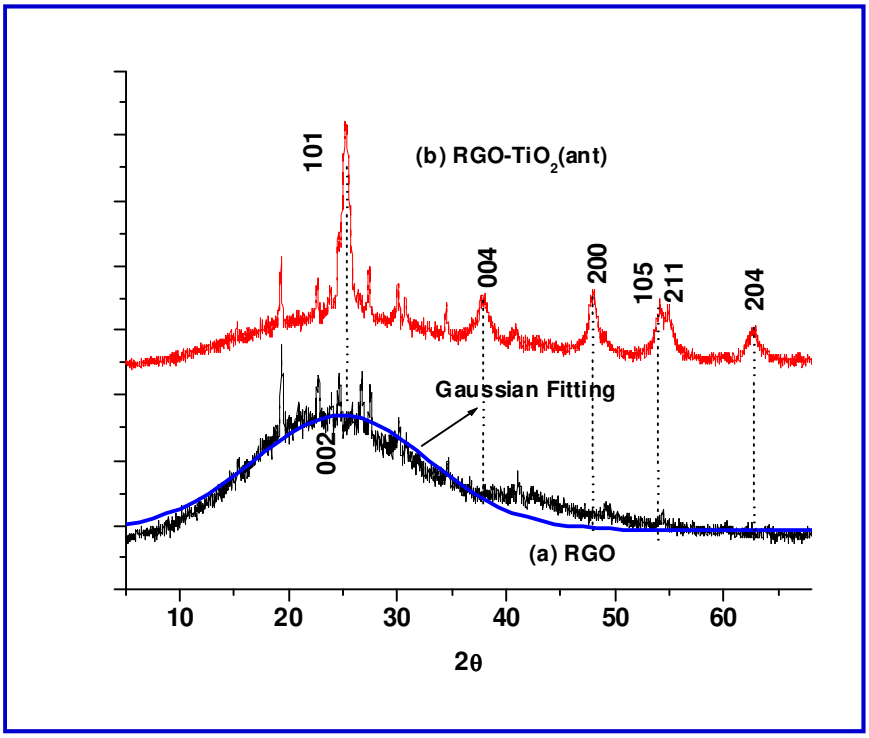

Figure 2

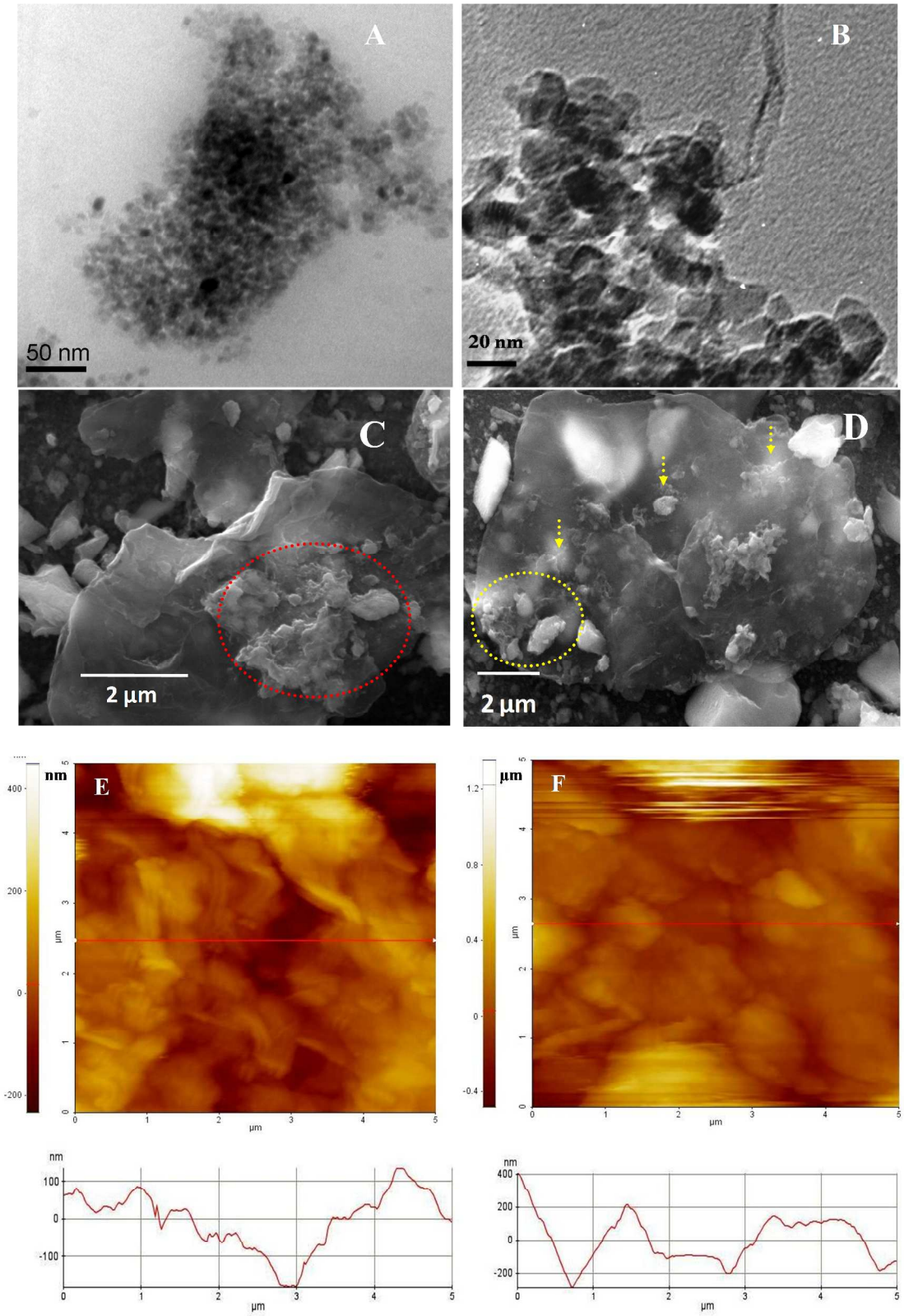

Figure 3

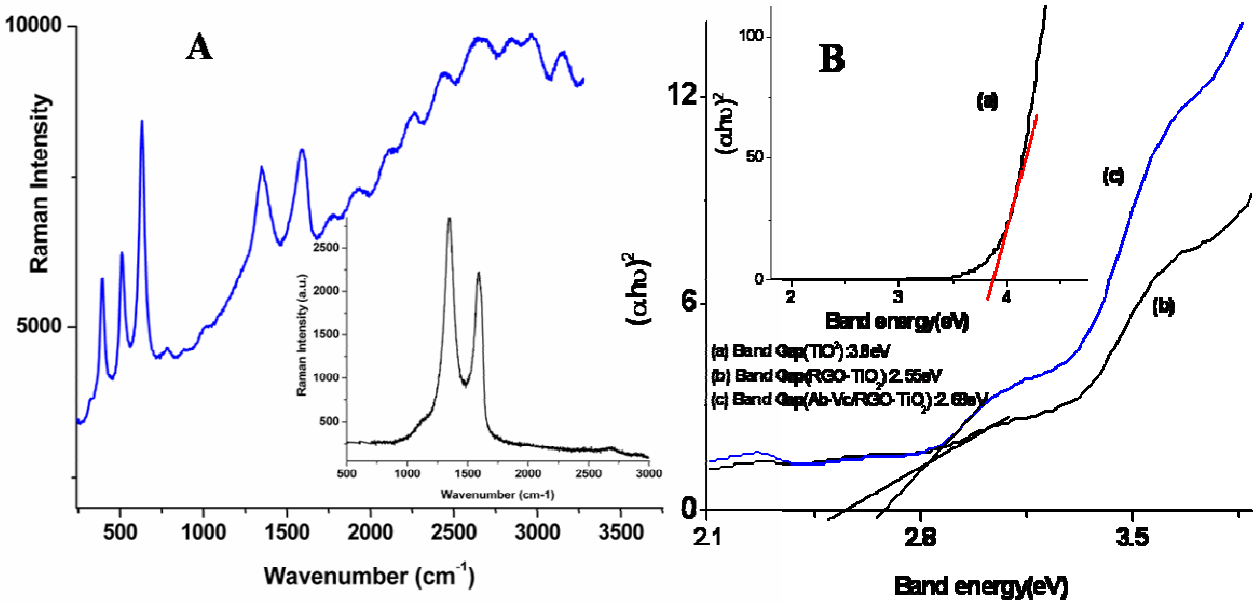

Figure 4 (A)

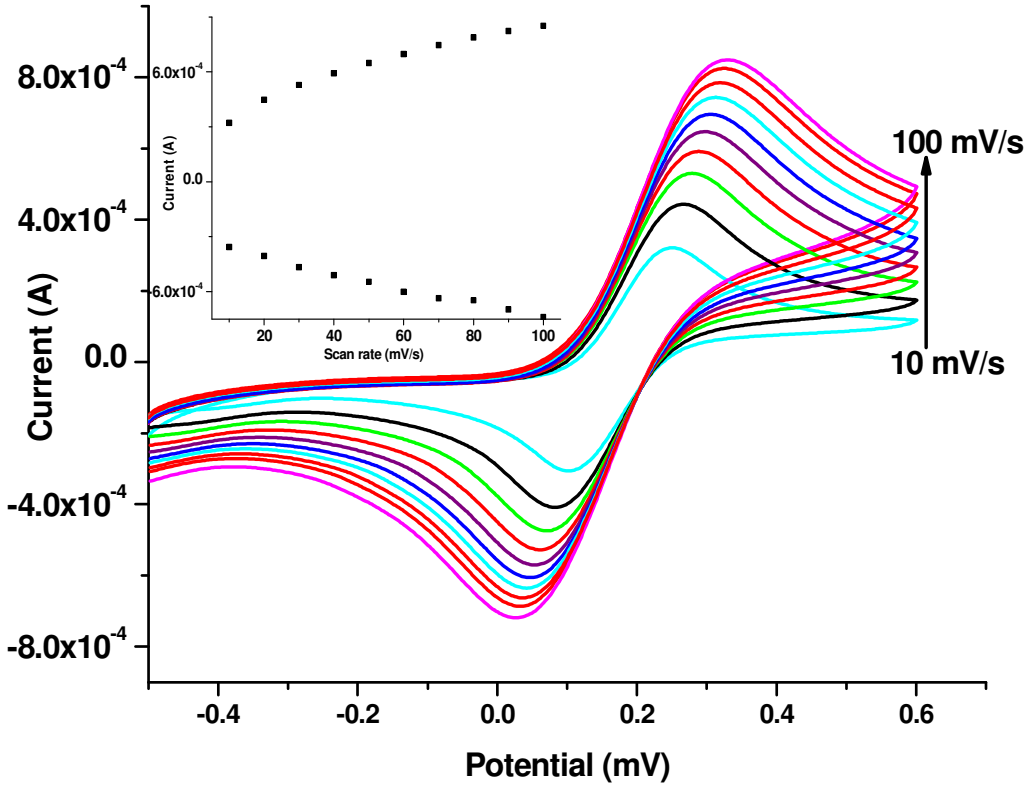

Figure 4 (B)

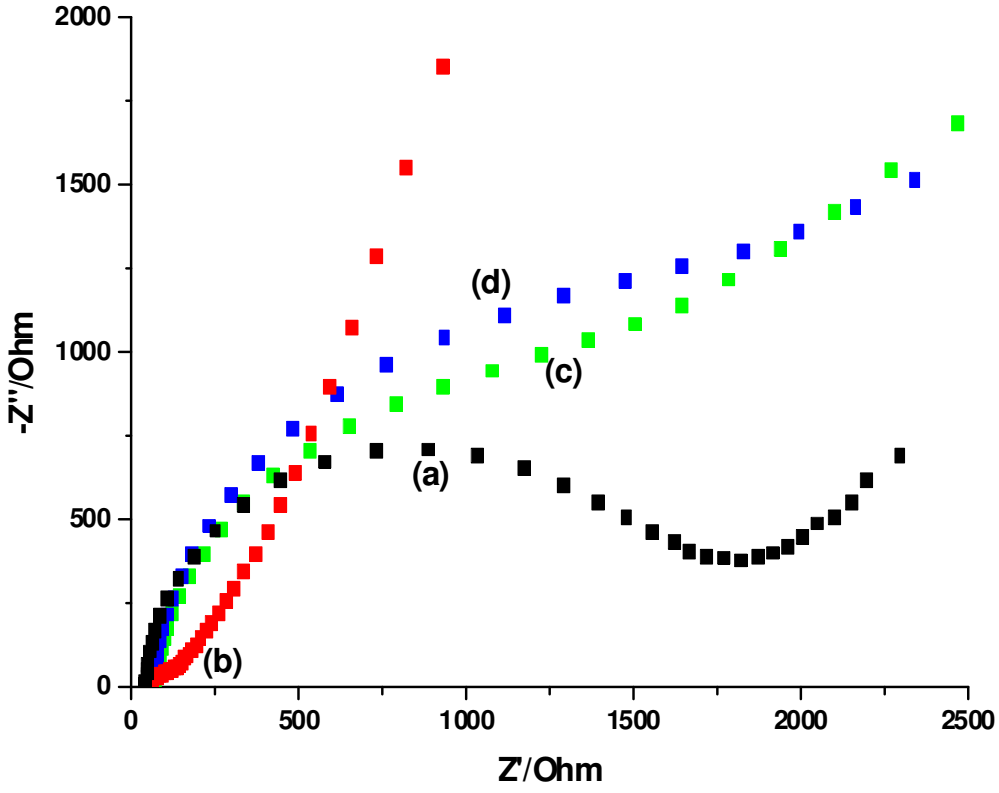

Figure 5 (A)

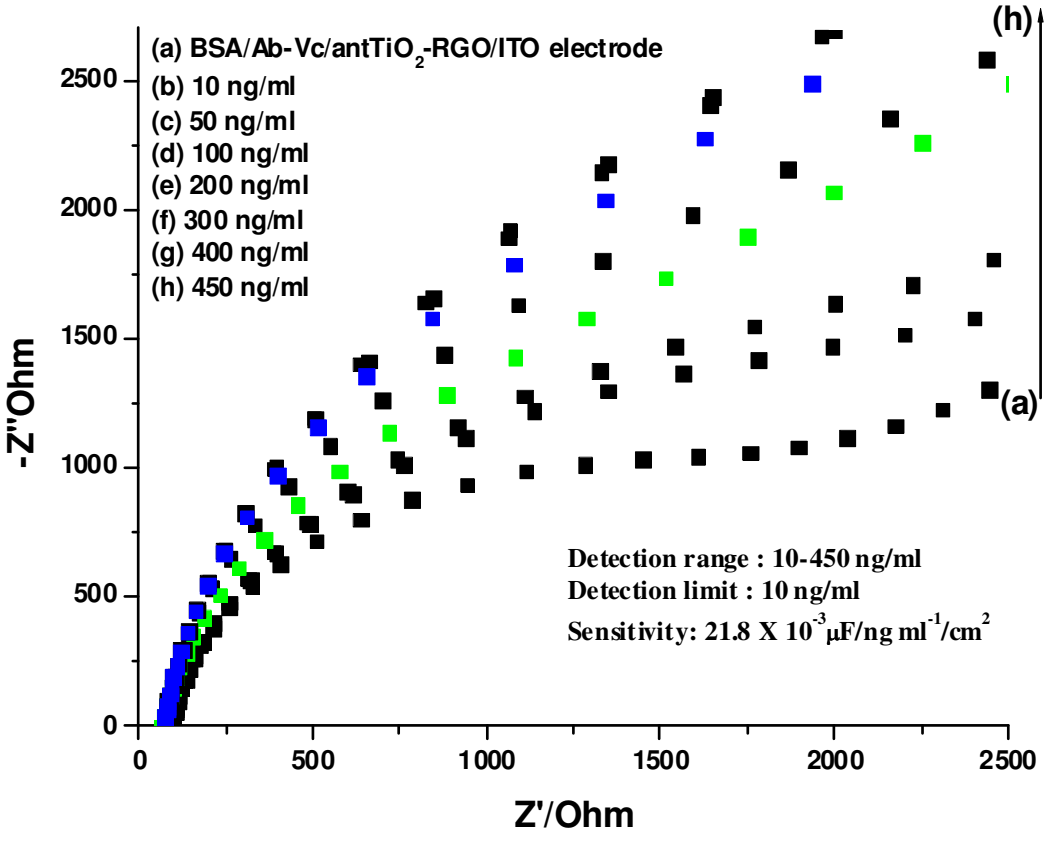

Figure 5 (B)

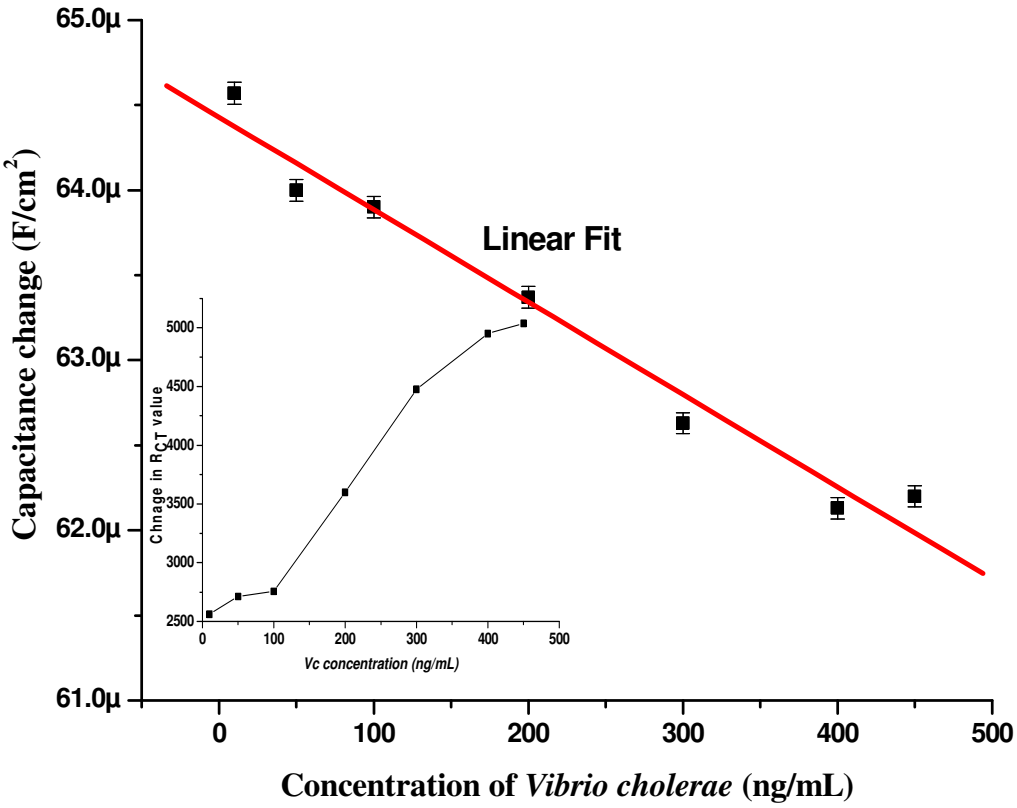

Figure 5 (C)

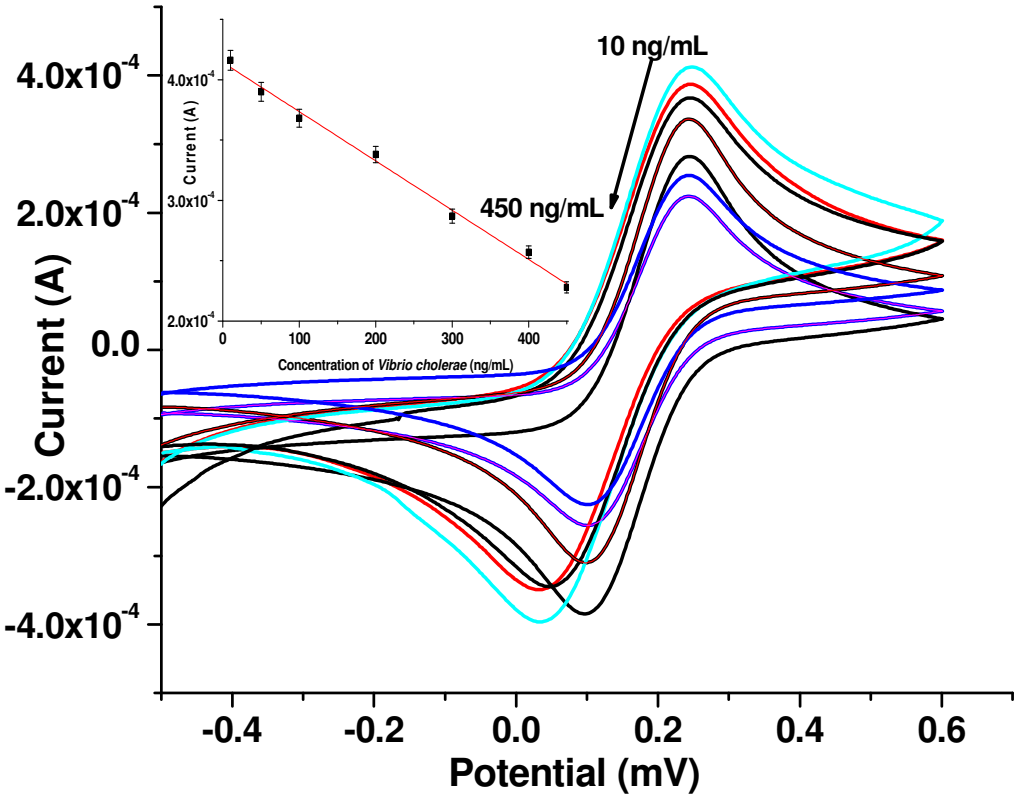

Table I. Equivalent circuit elements of different fabricated electrodes

Electrodes	R_s (Ω)	R_{CT} (kΩ)	C_{dl} (μF)	n
RGO-antTiO$_2$/ITO	-1.6×10^3	1.66	0.017	0.25
Ab-*Vc*/RGO-antTiO$_2$/ITO	7.06×10^1	2.28	0.668	0.89
BSA/Ab-*Vc*/RGO-antTiO$_2$/ITO	4.79×10^1	2.89	0.289	0.84